

## Calibration of Horizontal Acoustic Doppler Current profilers by three dimensional CFD simulations

Kari Bråtveit & Nils Reidar B. Olsen

To cite this article: Kari Bråtveit & Nils Reidar B. Olsen (2015) Calibration of Horizontal Acoustic Doppler Current profilers by three dimensional CFD simulations, Engineering Applications of Computational Fluid Mechanics, 9:1, 41-49, DOI: [10.1080/19942060.2015.1004807](https://doi.org/10.1080/19942060.2015.1004807)

To link to this article: <https://doi.org/10.1080/19942060.2015.1004807>



© 2015 The Author(s). Published by Taylor & Francis



Published online: 02 Mar 2015.



Submit your article to this journal [↗](#)



Article views: 747



View related articles [↗](#)



View Crossmark data [↗](#)

## Calibration of Horizontal Acoustic Doppler Current profilers by three dimensional CFD simulations

Kari Bråtveit\* and Nils Reidar B. Olsen

Department of Hydraulic and Environmental Engineering, The Norwegian University of Science and Technology, S.P. Andersens veg 5, N-7491 Trondheim, Norway

(Received 15 March 2014; final version received 17 September 2014)

This study presents a calibration method of horizontal acoustic Doppler current profilers (H-ADCP), based on 3D Computational Fluid Dynamics (CFD) simulations. Rigidly mounted H-ACCPs are currently used to continuously monitor water discharges. In this study three instruments were employed at separate sites in an unlined rock-blasted hydro power tunnel. The total discharge in the tunnel was predicted by fitting numerical and measured velocity profiles. The accuracy of the method was evaluated by comparing discharge predictions to results obtained by thermodynamic efficiency measurements. This study shows that 3D CFD simulations not only can be used to accurately calibrate H-ADCP, but also to assess the flow conditions at the locations of installation. An average error of 2% was obtained for the tunnel stretch that possessed the most uniform flow. However, the precision of the discharge estimates were confined by the CFD code's capability to correctly resolve the flow pattern.

**Keywords:** Hydro power; waterways; discharge; calibration of H-ADCP; numerical models

### 1. Introduction

Hydropower is an important renewable energy source worldwide, and 98% of the electric energy in Norway is hydroelectricity (Cheng, Shen, Wu, & Chau, 2012). A large portion of the waterways feeding the hydro power plants in Norway are unlined rock-blasted tunnels, making up a total distance of 3500 km. Many power plants are fed by multiple reservoirs and streams, and the system of tunnels can therefore be vast and complex. Reliable discharge data are crucial for water resource planning, since continuous series of water discharges are essential inputs both for hydrological models and operation simulations (McMillan, Freer, Pappenberger, Krueger, & Clark, 2010). Hence, an accurate monitoring system of the water discharges in the different branches of a tunnel system is valuable.

The current article presents an approach where H-ADCP instruments are applied in a hydro power tunnel. The transducers on an H-ADCP transmit acoustic signals in horizontal lines. These signals are reflected by suspended particles in the flow, and the Doppler effects can be utilized to calculate the water velocities. A two beam H-ADCP measures the flow velocities in two horizontal lines. The beam velocities are transposed into one horizontal velocity profile. Since the H-ADCP does not measure the velocity distribution over the whole cross section, it needs to be calibrated in order to determine the discharge.

In this study a calibration procedure founded on 3D CFD simulations is suggested. A 3D CFD model can

be used to compute the velocities and the corresponding discharges. Thus, the total discharge can be predicted based on the best fit between measured and computed velocity profiles. The main advantage of utilizing a 3D numerical approach is that it enables a more detailed evaluation of how a complex geometry affects the flow field, because a 3D CFD simulation provides an estimate of the spatial variation of the velocities. In order to compare the accuracy of resulting CFD discharges, a secondary field measurement was conducted. The secondary discharge measurement was part of a conventional thermodynamic efficiency measurement.

Recent studies described how H-ADCP can be calibrated and employed to continuously monitor river discharge (Nihei & Kimizu, 2008; Sassi, Hoitink, Vermeulen, & Hidayat, 2011). Often the discharge is found by applying the index-velocity method. The index velocity method normally computes the discharge by two separate ratings, the index velocity rating and the stage-area rating. The mean channel velocity and the cross-sectional area are then multiplied together to compute the discharge. The mean channel velocity is a function of the streamwise velocity, stage, cross-stream velocity and velocity head. In a pressurized flow system the water filled area will be constant, which eliminates the need of establishing a stage-area rating curve. The index-rating is established by regression, where the relationship between the mean cross-sectional velocity for the standard section and the

\*Corresponding author. Email: [kari.bratveit@ntnu.no](mailto:kari.bratveit@ntnu.no)

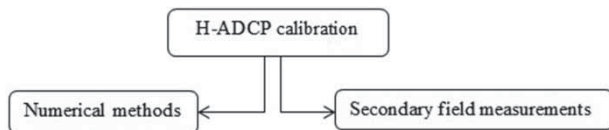


Figure 1. Calibration methods of ADCPs.

measured index velocity is defined (Gandhi, Verma, & Patnaik, 2008; Levesque & Osberg, 2012). The index velocity rating must be developed through a calibration process. This calibration process can be divided into two main categories; numerical methods or secondary field measurements, as illustrated in Figure 1. In most operated flows several discharge levels can be determined by secondary field measurements. In contrast, numerical methods become useful for natural flows and flows in structures that are dangerous to access for field measurements. However, a reliable relationship between the velocities and discharge is sometimes hard to establish, regardless of the method chosen, for example, for flood events.

This issue has been resolved in different ways. An automatic system that changes the vertical position of the H-ADCPs, and in this way collects the velocities for the entire cross section, has been developed. However, such a system is expensive and spacious. Another method applied is to interpolate and extrapolate the horizontal velocity profile or point velocity measurements over the whole cross section on the basis of the law of the wall (Gandhi, Verma, & Patnaik, 2008; Nihei & Kimizu, 2008). However, the law of the wall is only valid for a steady, uniform and fully developed turbulent flow, and does not capture the dynamic principle for fluid motion. The accuracy of this approach therefore decreases distinctly (Nihei & Kimizu, 2006).

The most recently developed calibration method is based on assimilating a river flow simulation to H-ADCP field data. Assimilations of river flow data are infrequently performed (Sulzer, Rutschmann, & Kinzelbach, 2002). However, Nihei and Kimizu (2006) have developed a river flow model that incorporates the measured velocities across a horizontal line at a fixed height. In these numerical simulations the measured velocity profiles are interpolated and extrapolated over the cross section. This method is referred to as the dynamic interpolation and extrapolation method (DIEX). The fundamental equation in a DIEX simulation calculates the velocity field in the cross-sectional domain. The equation is a simplified version of the two-dimensional momentum equation. In order to solve the equation a zero-equation-turbulence model is applied (Nihei & Kimizu, 2008).

In this study, a new calibration method has been tested. This method is based on determining the flow field by 3D CFD simulations. This has earlier been done by Olsen and Kjellesvig (1999), who computed flow in a desilting basin of the Svartisen Hydropower plant in Norway. Recently a number of numerical studies have been conducted where

CFD is used to predict the flow fields for different hydraulic cases, as documented by Baghalian, Bonakdari, Nazari, and Fazil (2012), Haun, Olsen, and Feurich (2011), Chau and Jiang (2004), Andersson, Andreasson, and Lundström (2013), Erduran, Seckin, Kocaman, and Atabay (2012), Chau and Jiang (2001), and Baranya, Olsen, Stoesser, and Sturm (2012).

A detailed 3D numerical model incorporates the fluid-structure interaction, and enables an evaluation of the cross-stream velocities. In the presented study, the computations were performed by the commercial 3D CFD package, Star-CCM+. This numerical application can solve the Reynolds-averaged Navier-Stokes (CD-adapco, 2009), equation with a standard two equation  $k-\epsilon$  turbulence model (Haun, Olsen, & Feurich, 2011). A  $k-\epsilon$  model computes the turbulent eddy-viscosity by solving two partial differential equations. A  $k-\epsilon$  turbulence model requires no calibrations contrary to a zero-equation model.

## 2. Measurements

### 2.1. Study site

This study was conducted in a fully pressurized rock-blasted unlined hydro power tunnel, which is part of the supply system of Tonstad Hydro Power Plant; see Figure 2. Three 1200 kHz Broadband Channel master H-ADCPs from RDI were installed and deployed. During the measurements the section was pressurized with an approximately 60 meter water head. The water in this system was clear, the sediment concentration was low and few floating obstacles, such as fish or pieces of wood or plastic, were observed.

Each of the ADCPs was rigidly mounted to the tunnel wall at different locations. An overview of the geometry of the tunnel and the location of each instrument can be seen in Figure 3.

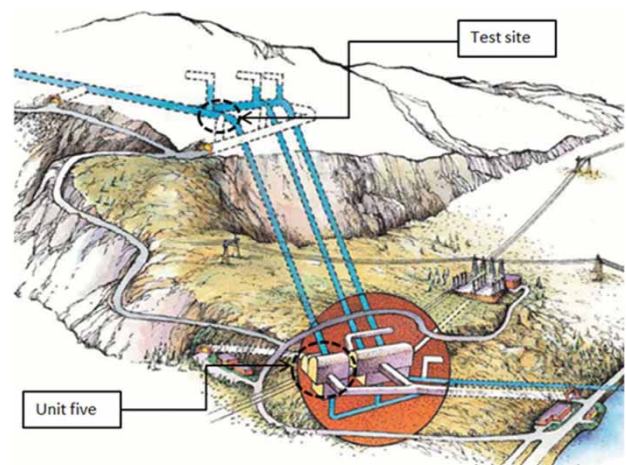


Figure 2. The lower part of Tonstad Hydro Power Plant (Helge Steinnes, 1993).



Figure 3. The location of the three ADCPs, top view. Flow direction is from right to left.

Power supply and data transfer were ensured through a cable connection to each of the instruments. The data were stored by a laptop located in a switchboard in the nearby access tunnel. Since the data from the vertical beam had no value this sensor was muted, which increased the transfer capacity. The cross section form and area of an unlined rock-blasted tunnel varies (Rønn & Skog, 1997). A 3D laser scan was performed to obtain correct geometry input for the CFD simulation. The details regarding scanning and generation of the surface mesh are presented by Bråtveit, Lia and Olsen (2012).

## 2.2. Field measurements

The ADCP measurements and the turbine efficiency measurement were conducted simultaneously at the fifth unit at Tonstad Hydro Power plant. The fifth turbine unit is located in one of the three branches of the conveyance tunnel system, i.e., downstream from the location of the three ADCPs, as seen in Figure 2. A standard procedure for turbine efficiency measurement was applied, and the unit was regulated stepwise at different outputs. For each step the production was kept constant for an adequate time period to ensure the flow had stabilized, and the transients were damped out. The four other units, two adjacent to each of the other two pressure shafts, were contra operated striving to maintain constant pressure and head loss in the system. The measuring program is presented in Table 1.

### 2.2.1. Thermodynamic efficiency measurement

During performance of a conventional TEM the turbine discharge has to be determined for each output. This type of measurement requires several instruments, such as thermometers, rotameters, pressure sensors and pulse counters.

Table 1. Measuring procedure and discharges obtained by TEM.

No.	Hour	Turbine Output [MW]	$Q_{\text{TEM}}$ [ $\text{m}^3/\text{s}$ ]
1	10:15	283,0	70,17
2	11:00	326,77	81,53
3	11:45	340,51	84,96
4	13:05	149,04	39,34
5	13:35	187,08	47,77
6	14:20	206,52	52,03
7	14:50	233,43	58,26

The thermometers and the pressure transducers are the most essential instruments regarding accurate determination of the discharge. Each of the measurements taken during the test included uncertainties, due to inaccuracy within the instrument used and random variations of the measured value. The individual biases were combined by the law of uncertainty propagation, and it was reported  $\pm 1.0\%$  of the actual discharge. The resulting discharges are provided in Table 1. Further details regarding the TEM can be found in Brænd (2013).

### 2.2.2. Velocity measurements by ADCP

The ADCP measurements were performed parallel to the TEM measurements. The water velocities were measured at each of the three locations by utilizing equal configuration for all sensors. An overview of the configuration used can be found in Table 2.

ADCP discharge measurements contain systematic and random errors, as in any other measurement. Main systematic errors arise due to biases in ADCP water velocity measurements, while the random errors are largely due to Doppler noise, or flow pulsations caused by turbulence (Huang, 2008). Random errors due to spatial resolution occur, since the velocities are measured radially, before being transformed into an orthogonal coordinate system by assuming that the flow between the two beams is horizontally homogeneous. Since the resulting velocities are spatially averaged, they are suspected to yield biases estimated of mean flow for highly three-dimensional flows (Nystrom, Oberg, & Rehmann, 2002). However, averaging the velocity data over a longer time period will reduce the random errors (Simpson, 2001). By choosing a long sampling time, the turbulence flow pattern will be averaged out (Muste, Yu, Pratt, & Abraham, 2002; Szupiany, Amsler, Best, & Parsons, 2007). The average interval in this study

Table 2. Set up configuration of ADCPs.

Specification	Quantity
Number of cells	50
Pings per ensemble	12
Depth cell length [cm]	25
Blank after transmit [cm]	10
Time between ensemble [s]	6

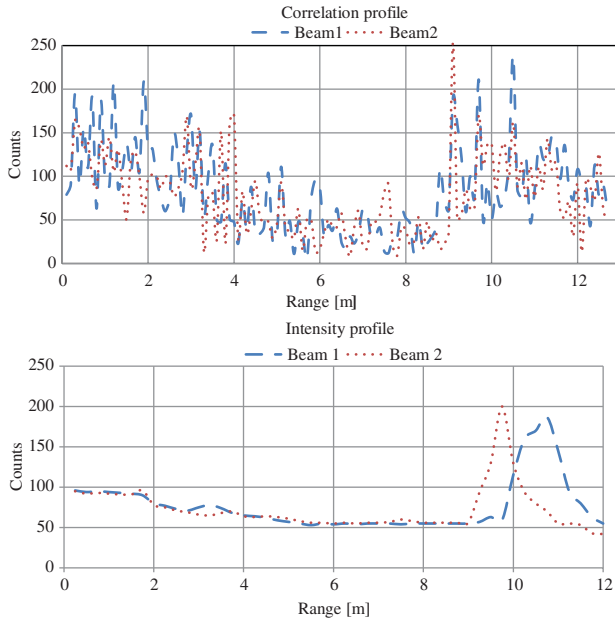


Figure 4. (a) Correlation profile and (b) Intensity profile from ADCP I at discharge level four.

was therefore set to 10 min, in order to reduce the uncertainty in the velocity data due to spatial resolution errors. The production output data were evaluated, and ADCP data were extracted for periods with stable production.

The quality of the recorded velocity data had to be evaluated to ensure that invalid data were excluded. The first limitation to consider was the width of the tunnel. Signals contaminated due to side lobbing from the opposite wall had to be excluded. For each of the three ADCPs, the intensity profile and correlation profile were evaluated. In Figure 4, two representative examples of these charts are presented by plots of values obtained from ADCP I. The location of the two peaks in the intensity profile, shown in Figure 4(b), reveals where the signals were reflected by the wall. Due to the roughness of the tunnel wall, the signals from the two beams hit the wall at different distances. Data that originated from bins located after the peak were removed. In addition this width was cut off by 6%, plus one bin size.

The second limitation considered was the correlation profile, as shown in Figure 4(a). The correlation count describes how well the returned signal corresponds to its original code tag. The data were only used if the data had a correlation factor above 72 (Teledyne, 2010). Finally, the echo intensity of the data was evaluated. Due to clear water the echo intensity profiles had very low values, as seen in Figure 4(b). The echo intensity profiles were obtained from the backscatter of the signal. A high-intensity count value indicates high sediment concentration (Moore, Coz, Hurther, & Paquier, 2011). It is known that the raw data include contamination caused by background or instrument noise (Levesque & Osberg, 2012). The Channel Masters noise

Table 3. Mean velocities and standard deviations obtained from ADCP measurements.

NO.	Hour	ADCP					
		I		II		III	
		$\bar{v}$ [m/s]	$\sigma_v$	$\bar{v}$ [m/s]	$\sigma_v$	$\bar{v}$ [m/s]	$\sigma_v$
1	10:15	1.2	0.56	0.56	0.10	0.51	0.09
2	11:00	1.3	0.58	0.66	0.11	0.59	0.09
3	11:45	1.2	0.69	0.69	0.12	0.64	0.10
4	13:05	0.7	0.31	0.30	0.06	0.28	0.06
5	13:35	0.7	0.41	0.36	0.08	0.33	0.07
6	14:20	1.0	0.36	0.42	0.08	0.39	0.07
7	14:50	1.1	0.47	0.47	0.09	0.44	0.08

level is assumed by RDI Teledyne to be around 40 counts. As seen in Figure 4(a) and 4(b) the intensity and correlation profiles have low counts values, and are decreasing into the expected noise level range of the instrument. Therefore, as a conservative assumption, the ADCP's velocity profiles are only considered valid up to five meters from the sensor, when operated in such clear water. The accuracy of the data was considered to be too low after five meters, due to the fact that the measured values were in the range of the background noise level. The resulting mean velocities for each output level, and the corresponding standard deviation are presented in Table 3.

### 2.3. Numerical modeling by CFD

The CFD simulations were performed by the commercial software STAR-CCM+, which is a CFD-package applied to a broad specter of physics. In this study the software was used to solve the Navier-Stokes equations in three dimensions. The boundary conditions of the model were set according to data obtained by field measurements, production rates, pressure, and temperature data were available. The computational domain was extended upstream of the inlet, in order to create a correct velocity distribution over the inlet. Though, after testing several different domains for the inlet structure the velocity distributions downstream the inlet remained nearly identical. It seems to be governed by the flow separation caused by the rapid expansion 11.2 m downstream the inlet. Both first- and second-order discretization schemes were tested, but little variance in the results was found. Therefore a first order discretization scheme was used for the convective terms. For each output level several CFD simulations were conducted.

A turbulent flow is characterized by a large variation in scales of motions, and an accurate numerical approximation of a turbulent flow field involves resolving these equations for all scales of motion. The optimum way to do that is to perform a Direct Numerical Simulation (DNS) (Wissink, 1995). However, for flows with high Reynolds numbers a DNS simulation requires that the size of the numerical mesh is smaller than the size of small-turbulent

motions, where dissipation takes place. As a consequent, the number of grid points are needed for most practical hydraulic engineering problems becomes so large that computational resources necessary exceed the capacity of available computers (Rodi, Conatantinescu, & Stoesser, 2013). A common way to avoid massive computations is to use a turbulence model based on the Reynolds average Navier-Stokes Equations – a so called RANS model. A RANS model is based on averaging the NS equations in time, meaning that this statistical model accounts for the entire effect of the turbulence motions. In the last decades the computer power has kept increasing, and this has revealed that RANS models have limitations, especially when applied for coherent structures. Recent development has provided methods such as Large Eddy Simulations (LES), where the large scales are resolved and the small scales are model (Rodi, Conatantinescu, & Stoesser, 2013). Another recent method is the Detached Eddy Simulation (DES), which is a hybrid modeling approach where RANS closure is applied in some parts of the flow field and LES in others (CD-adapco, 2009). However, LES and DES methods demand a highly dense grid to correctly resolve the dissipation, while RANS simulations can be computed based on coarser grids. Hence, RANS models are most applicable for practical employment, because

they are economical in terms of computational and memory resources. Though, one should be aware that RANS simulations have limitations, especially when dealing with large-scale turbulence structures (Rodi, Conatantinescu, & Stoesser, 2013).

The calibration method suggested here is based upon utilizing a RANS model applying a standard  $k-\varepsilon$  turbulence model with a high Reynolds number wall treatment. A  $k-\varepsilon$  model is a two-equation model used to estimate the eddy viscosity by relating the mean-flow quantities to the time scales of turbulence. Further details of this study can be found in Bråtveit, Brevik, & Olsen (2013).

Verification of a CFD simulation involves a systematic mesh refinement study (Versteeg & Malalasekera, 2007). Hence, several types of nonorthogonal unstructured grids were generated from the surface mesh. Grids based on both orthogonal hexahedral and polyhedral cells were applied, and the grids were refined from the wall to the centre of the tunnel. Grid-dependency tests were performed throughout, including refinements of the grids in the expansion zone downstream the inlet. Once a grid independent solution was obtained, a final test of CFD model was performed by comparing the output to experimental data (Versteeg & Malalasekera, 2007). The final grid chosen for calibration consisted of 849 627 hexahedral cells, which represents a

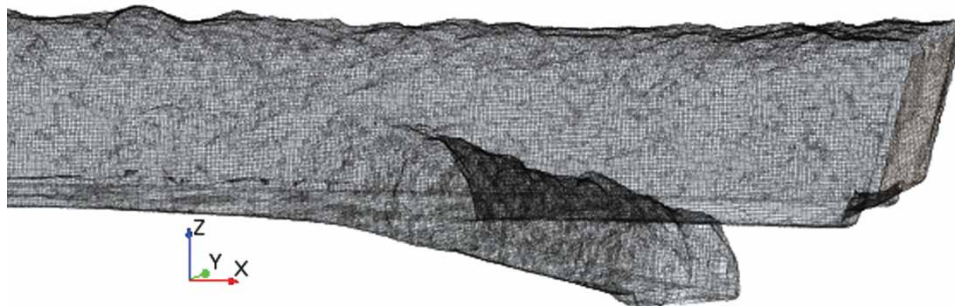


Figure 5. The volume mesh consisted of trimmed cells.

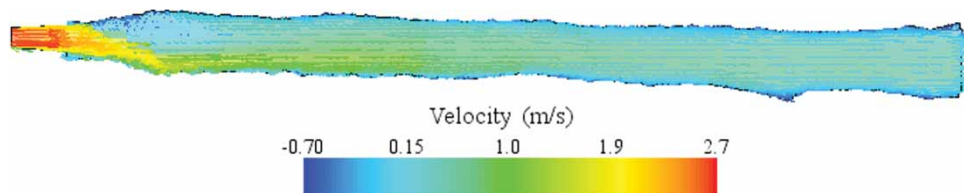


Figure 6. Streamwise velocities plotted for the central plan of the structure.

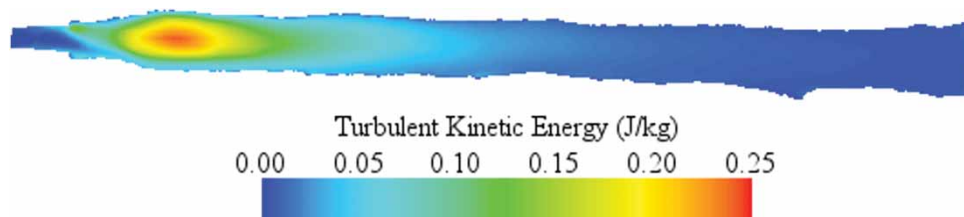


Figure 7. TKE values from simulation of discharge level one.

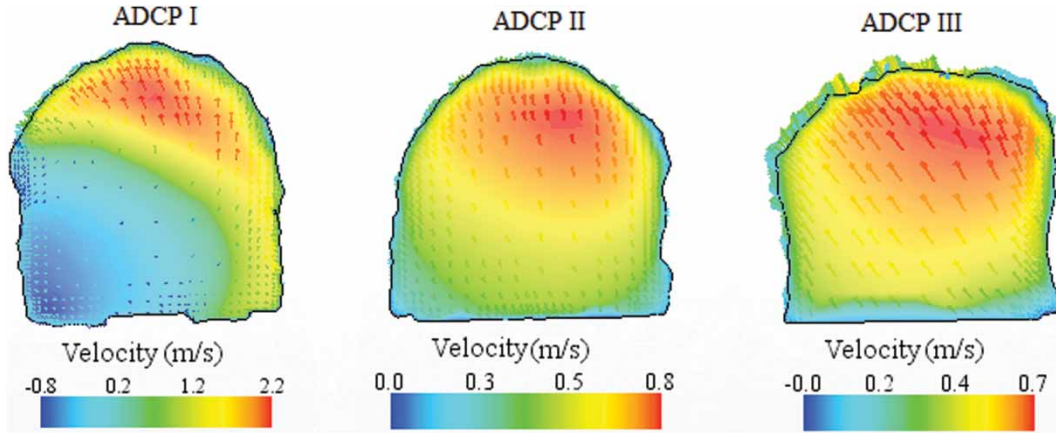


Figure 8. Velocity distributions at different cross sections.

volume mesh of intermediate size, possible to run on an ordinary off-the-shelf computer. A plot of this relatively coarse mesh is provided in Figure 5.

### 3. Results and discussion

The model evaluation techniques applied in this study include both graphical and statistical methods. First, the

flow pattern occurring in the structure was assessed graphically. This is useful because it allows us to evaluate the impact of the geometry on the flow. Figure 6 shows a representative plot of the flow field for the first discharge level in the stream-wise direction for the central plane of the structure. In Figure 7 the corresponding turbulent kinetic energy (TKE) values for the same plane are shown, while plots of the velocity distribution over the cross sections where the instruments are located are provided in Figure 8. The plots indicate that a recirculation zone develops downstream the rapid expansion of the inlet structure, causing increased TKE values in the first part of the tunnel. The plots of the velocity distributions for the cross sections show that the flow field changes from skewed at ADCP I toward more uniform at ADCP II and ADCP III.

The velocity profiles obtained by CFD were graphically compared to the ADCP profiles. One chart was created for each sensor at each discharge level. An example of these plots, obtained from the iteration process for output level one, can be seen in Figure 9. The filtering process previously executed indicated that only the first five meters of the measured profiles are valid, and therefore used for comparison. The graphical evaluation of the numerical simulations reveals that the CFD simulation fails to predict the flow pattern correctly for the first part of the structure, i.e., the simulated velocity profiles obtained for ADCP I do not resemble the profiles from the field measurements. This ADCP is located shortly downstream from an expansion

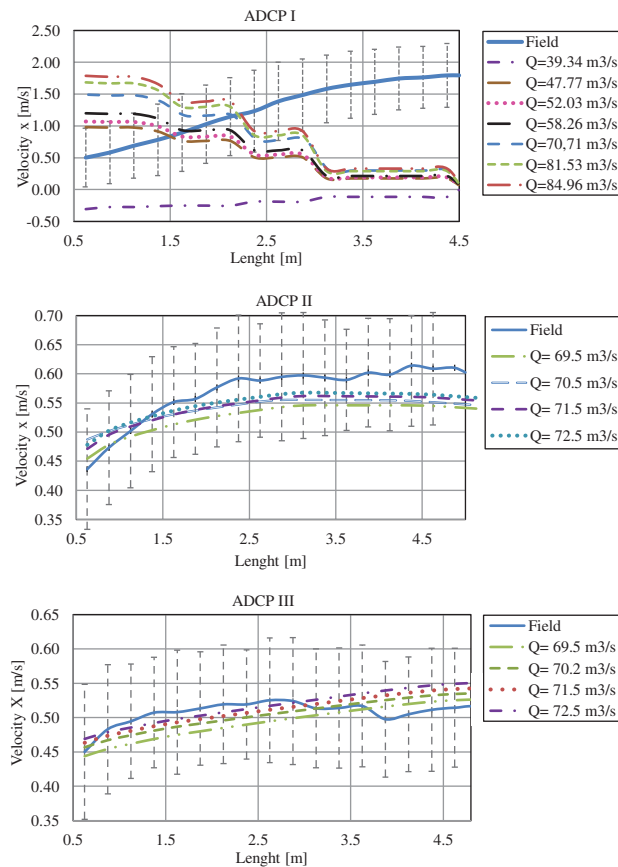


Figure 9. Velocity plots obtained by field measurements and simulation (a) ADCP I; (b) ADCP II; (c) ADCP III.

Table 4. Discharges and statistics obtained during the iteration process of discharge level one for ADCP III.

Iteration	Profile III			
	$Q_i$ [m <sup>3</sup> /s]	SSE	RMSE	PBIAS
1	69.5	0.01	0.03	2.1
2	71.5	0.01	0.02	-1.3
3	72.5	0.01	0.03	-2.6
4	70.16	0.01	0.02	0.0

Table 5. Results from the statistical evaluation.

No.	Profile II				Profile III			
	Qi [m <sup>3</sup> /s]	SSE	RMSE	PBIAS	Qi [m <sup>3</sup> /s]	SSE	RMSE	PBIAS
1	73.91	0.01	0.02	0.7	70.16	0.01	0.02	0.0
2	87.75	0.01	0.02	0.5	82.39	0.15	0.02	0.4
3	91.69	0.03	0.04	0.05	89.63	0.01	0.02	0.0
4	41.00	0.00	0.01	0.0	38.83	1.85	0.31	0.1
5	48.90	0.00	0.010	0.3	46.70	0.00	0.01	0.0
6	56.43	0.01	0.02	0.0	55.39	0.00	0.01	0.0
7	63.96	0.00	0.02	0.0	61.29	0.01	0.02	0.0

Table 6. Comparison of the discharge values.

No.	Q <sub>TEM</sub> [m <sup>3</sup> /s]	Q <sub>II</sub> CFD [m <sup>3</sup> /s]	Q <sub>III</sub> CFD [m <sup>3</sup> /s]	Error Q <sub>II</sub> [%]	Error Q <sub>III</sub> [%]	TKE II [J/kg]	TKE III [J/kg]
1	70.17	75	70.16	6.9	0.0	0.014	0.007
2	81.53	87.75	82.39	7.6	1.1	0.022	0.010
3	84.96	91.69	89.63	8.0	5.6	0.026	0.011
4	39.34	41	38.83	4.2	-1.3	0.004	0.002
5	47.77	48.9	46.7	2.4	-2.2	0.005	0.002
6	52.03	56.43	55.39	8.5	6.5	0.008	0.004
7	58.26	63.96	61.29	9.8	5.2	0.010	0.004

zone, where the flow is highly unsteady. Figure 9(a) shows that two RANS simulations with nearly identical boundary conditions can yield recirculation zones occurring on opposite side downstream from a rapid expansion. In this case the recirculation zones occurred randomly on the left or the right side of the structure. The velocity profiles for ADCP II and ADCP III fit relatively well, indicating that the CFD simulations were able to estimate the flow conditions fairly well.

Several commonly used statistical error indicators were applied in order to evaluate the fit between the simulated and the calculated velocities during the iteration process. The statistical evaluation includes comparing means, standard square error (SSE), root mean square error (RMSE) and percent bias (PBIAS) (Moriasi et al., 2007). The equation for SSE, RMSE and PBIAS are presented below. Only ADCP II and ADCP III were statistically evaluated, since the graphical evaluation revealed unsatisfactory correlation for ADCP I.

$$SSE = \sum_{i=1}^n (Y_i^{obs} - Y_i^{sim})^2 \quad (10)$$

$$RMSE = \sqrt{\frac{\sum_{i=1}^n (x_{obs,i} - x_{sim,i})^2}{n}} \quad (11)$$

$$PBIAS = \left[ \frac{\sum_{i=1}^n (Y_i^{obs} - Y_i^{sim}) \times (100)}{\sum_{i=1}^n (Y_i^{obs})} \right] \quad (12)$$

The various discharge values obtained during the iteration process for ADCP III at output level one are presented in Table 4. Similar iteration processes have been conducted for each of the seven discharge levels for both ADCP II and

Table 7. Resulting fit obtained regression analysis.

ADCP No.	R <sup>2</sup> value A)	R <sup>2</sup> value B)
I	0,9609	—
II	0,9735	0,9706
III	0,9900	0,9900

ADCP III. The final results from these iterations are provided in Table 5. It can be observed that the SSE, RMSE and PBIAS values in general are low, but they increase for higher discharges. The discharge values obtained by CFD, Q<sub>CFD</sub>, are compared against the TEM discharges, and the percent errors between the values were calculated. These results are listed in Table 6. The iteration process shows that the PBIAS values and the errors are lowest for ADCP III, where the TKE values are lowest. The results reveal that the accuracy of the discharges obtained by CFD are restricted by the levels of turbulence arising at the specific site of installation, and that a RANS simulation is not able to predict the flow field close to a rapid expansion correctly.

Finally, the index velocity ratings for each of the sensors were established by regression. Two types of regressions were performed, (A) between Q<sub>TEM</sub> values and the corresponding mean ADCP velocities, and (B) between Q<sub>CFD</sub> values and the corresponding mean ADCP velocities. The R squared values are presented in Table 7. It can be observed that coefficients of determinations are higher for ADCP III than for ADCP II.

#### 4. Conclusion

In this study, a calibration method for rigidly mounted H-ADCPs based on results from 3D CFD simulations is

evaluated. The study shows that detailed CFD simulations provide valuable insight into the flow pattern and the turbulence level arising in different parts of the structure. This is essential information, not only to ensure accurate calibration, but also for deciding the best site of installation for the ADCPs.

One of the well-known limitations of H-ADCP is that the instruments yield only a narrow representative line of the cross section's velocity distribution. Hence, it becomes crucial to apply the instrument so that the measured line captures the changes in the discharge. Locations where the cross sectional velocity distribution is fairly uniform, and not largely influenced by secondary currents, are therefore preferred. In future work, it is of interest to investigate the accuracy of instruments installed at different locations in the same cross-section. For example, comparing results obtained from vertical compared to horizontal position sensors.

A RANS model is economical in terms of memory and computational cost, but has limitations when large-scale turbulence structures dominate the flow. This study shows that a RANS simulation with a standard  $k-\epsilon$  model was not able to correctly resolve the flow pattern close to a rapid expansion. Though, it was found that the precision of the flow field increased parallel to the reduction in turbulent kinetic energy. Hence, the accuracy of the calibration method was found confined by the level of turbulence occurring at the locations of the sensors, and the CFD's code capability to correctly resolve the flow pattern.

The simulated discharges were compared to values obtained by TEM. An average error of  $\pm 2\%$  was found for the ADCP applied at the tunnel stretch with the most uniform flow condition. This error is in the range of the accuracy of the instruments.

This study shows that H-ADCP calibrated with CFD simulations can yield accurate and continual discharge measurements for pressurized hydro tunnels. Prediction of the flow field can be established by performing economical RANS simulations with standard  $k-\epsilon$  models. Though, it should be kept in mind that RANS simulations have difficulties in coping adequately with complex flow phenomena, such as large-scale turbulence structures Rodi, Conatantinescu, & Stoesser, 2013), and one should strive to avoid installing the instrument in or close to recirculation zones.

### Acknowledgements

This study is funded by the Centre for Environmental Design of Renewable Energy (CEDREN) in Norway. The writers are grateful to Sira-Kvina Kraftselskap A/S for technical support, facilitating access and willingness in cooperation. A. Sæterdal, K. Grangier, G. Brænd and Å. Killingveit have provided useful support. We also want to thank NOTUR for providing computational time on the Vilje HPC cluster.

### References

- Andersson, A. G., Andreasson, P., & Lundström, T. S. (2013). CFD-modelling and validation of free surface flow during spilling of reservoir in down-scale model. *Engineering Applications of Computational Fluid Mechanics*, 7(1), 159–167.
- Baghalian, S., Bonakdari, H., Nazari, F., & Fazil, M. (2012). Closed-form solution for flow field in curved channels in comparison with experimental and numerical analyses and artificial neural network. *Engineering Applications of Computational Fluid Mechanics*, 6(4), 514–526.
- Baranya, S., Olsen, N. R. B., Stoesser, T., & Sturm, T. (2012). Three-dimensional rans modeling of flow around circular piers using nested grids. *Engineering Applications of Computational Fluid Mechanics*, 6(4), 648–662.
- Brænd, G. (2013). *Tonstad kraftverk Virkingsgradsmålinger turbin 5*. Norway: Report, SWECO.
- Bråtveit, K., Brevik, O., & Olsen, N. R. B. (2013). *Three dimensional numerical study of an unlined pressurized rock-blasted sand trap*. 35th IAHR World Congress, Chengdu, China.
- Bråtveit, K., Lia, L., & Olsen, N. R. B. (2012). An efficient method to describe the geometry and the roughness of an existing unlined hydro power tunnel. *Energy Procedia*, 20, 200–206.
- CD-adapco. (2009). *User Guide STAR-CCM+ Version 4.06.011*. CD-adapco.
- Chau, K. W., & Jiang, Y. W. (2001). 3D numerical model for Pearl River Estuary. *Journal of Hydraulic Engineering*, 127(1), 72–82.
- Chau, K. W., & Jiang, Y. W. (2004). A three-dimensional pollutant transport model in orthogonal curvilinear and sigma coordinate system for Pearl river estuary. *International Journal of Environment and Pollution*, 21(2), 188–198.
- Cheng, C. T., Shen, J. J., Wu, X. Y., & Chau, K. W. (2012). Operation challenges for fast-growing China's hydropower systems and response to energy saving and emission reduction. *Renewable and Sustainable Energy Reviews*, 16(5), 2386–2393.
- Erduran, K. S., Seckin, G., Kocaman, S., & Atabay, S. (2012). 3D numerical modelling of flow around skewed bridge crossing. *Engineering Applications of Computational Fluid Mechanics*, 6(3), 475–489.
- Gandhi, B. K., Verma, H. K., & Patnaik, S. S. (2008). *Discharge measurement in small hydropower stations using Acoustic Doppler Current Profiler*. 7th International Group of Hydraulic Efficiency Measurement, Milano, Italy.
- Haun, S., Olsen, N. R. B., & Feurich, R. (2011). Numerical modeling of flow over trapezoidal broad-crested weir. *Engineering Applications of Computational Fluid Mechanics*, 5(3), 397–405.
- Huang, H. (2008). *Estimating precision of moving boat ADCP discharge measurement*. Australian Hydrographers Association Conference 2008; Canberra, Australia.
- Levesque, V. A., & Osberg, K. A. (2012). *Computing discharge using the Index Velocity method, techniques and methods 3-A23*. Reston, VA: U.S. Department of The Interior, United States Geological Survey.
- McMillan, H., Freer, J., Pappenberger, F., Krueger, T., & Clark, M. (2010). Impacts of uncertain river flow data on rainfall-runoff model calibration and discharge predictions. *Hydrological Processes*, 24(10), 1270–1284.
- Moore, S. A., Coz, L. J., Hurther, D., & Paquier, A. (2011). *On the use of Horizontal-ADCPs for Sediment Flux Measurements in Rivers*. 34th IAHR World Congress, Brisbane, Australia.

- Moriasi, D. N., Arnold, J. G., Van Liew, M. W., Bingner, R. L., Harmel, R. D., & Veith, T. L. (2007). Model Evaluation guidelines for systematic quantification of accuracy in watershed simulations. *American Society of Agricultural and Biological Engineers*, 50(3), 885–900.
- Muste, M., Yu, K., Pratt, T. C., & Abraham, D. (2002). ADCP measurements at fixed river locations. In *Hydraulic measurements and experimental methods 2002(CD-ROM) ASCE* (pp. 622–633). Estes Park, CO.
- Nihei, Y., & Kimizu, A. (2006). Evaluation of river velocity and discharge with a new assimilated method. *International Journal of River Basin Management*, 4(1), 27–30.
- Nihei, Y., & Kimizu, A. (2008). A new monitoring system for river discharge with horizontal acoustic Doppler current profiler measurements and river flow simulation. *Water Resources Research*, 44(4), W00D20.
- Nystrom, E. A., Oberg, K. A., & Rehmann, C. R. (2002). Measurement of turbulence with acoustic Doppler current profilers—Sources of error and laboratory results. In *Hydraulic Measurements & Experimental Methods 2002 (CD-ROM) ASCE* (pp. 346–355). Estes Park, CO.
- Olsen, N. R. B., & Kjellesvig, H. M. (1999). Three-dimensional numerical modelling of bed changes in a sand trap. *Journal of Hydraulic Research*, 37(2), 189–198.
- Rodi, W., Conatantinescu, G., & Stoesser, T. (2013). *Large Eddy simulation in hydraulics*. Netherlands: Book, CRC Press/Balkema.
- Rønn, P. E., & Skog, M. (1997). *New method for estimation of head loss in unlined water tunnels*. Proceedings of the 3th International Conference on Hydro power Hydropower'97, Trondheim, Norway.
- Sassi, M. G., Hoitink, A. J. F., Vermeulen, B., & Hidayat (2011). *Discharge estimation from H-ADCP measurements in a tidal river subject to sidewall effects and a mobile bed*. *Water Resources Research*, 47(6), W06504.
- Simpson, M. R. (2001). *Discharge measurements using a broad-band Acoustic Doppler Current Profile* (Open-file report 01-1). Sacramento, CA: United States Geological Survey.
- Sulzer, S., Rutschmann, P., & Kinzelbach, W. (2002). Flood discharge prediction using two-dimensional inverse modeling. *Journal of Hydraulic Engineering*, 128(1), 46–54.
- Szupiany, R. N., Amsler, M. L., Best, J. L., & Parsons, D. R. (2007). Comparison of fixed- and moving-vessel flow measurements with an aDp in a large river. *Journal of Hydraulic Engineering*, 133(12), 1299–1309.
- Teledyne, R. D. I. (2010). *ADCP coordinate transformation, formulas and calculations*. User's manual, RDI Teledyne, San Diego, USA.
- Versteeg, H. K., & Malalasekera, W. (2007). *An introduction to computational fluid dynamics. The finite volume method* (2nd ed.). Essex, UK: Person Education.
- Wissink, J. G. (1995). *Direct numerical simulations of turbulence*. Netherlands: Proefschrift, Rijksuniversiteit Groningen.